Continuous Approximation of Shellular Funicular Structures

Mostafa Akbari[*,a], Masoud Akbarzadeh[a,b]

[*,a] Polyhedral Structures Laboratory, Weitzman School of Design, University of Pennsylvania, Philadelphia, USA
Pennovation Center, 3401 Grays Ferry Ave. Philadelphia, PA, 19146

[b]General Robotic, Automation, Sensing and Perception (GRASP) Lab, School of Engineering and Applied
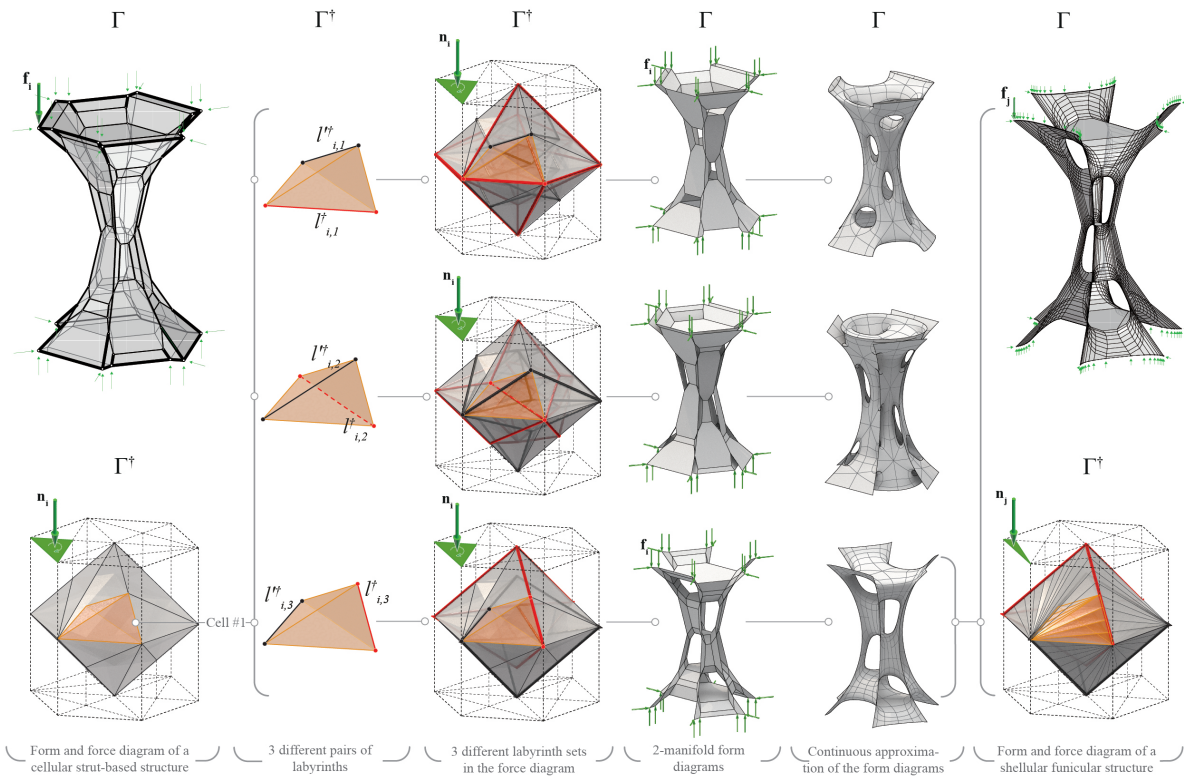Science, University of Pennsylvania, Philadelphia, USA

Figure 1: Graphical abstract; the process of designing the geometry of shellular funicular structures and approximating it using catmull-clark algorithm.

Abstract:

This paper introduces an interactive form finding technique to design and explore continuous Shellular Funicular Structures in the context of Polyhedral Graphic Statics (PGS). Shellular funicular forms are two-manifold shell-based geometries dividing the space into two interwoven sub-spaces, each of which can be represented by a 3D graph named labyrinth [1]. Both form and force diagrams include labyrinths
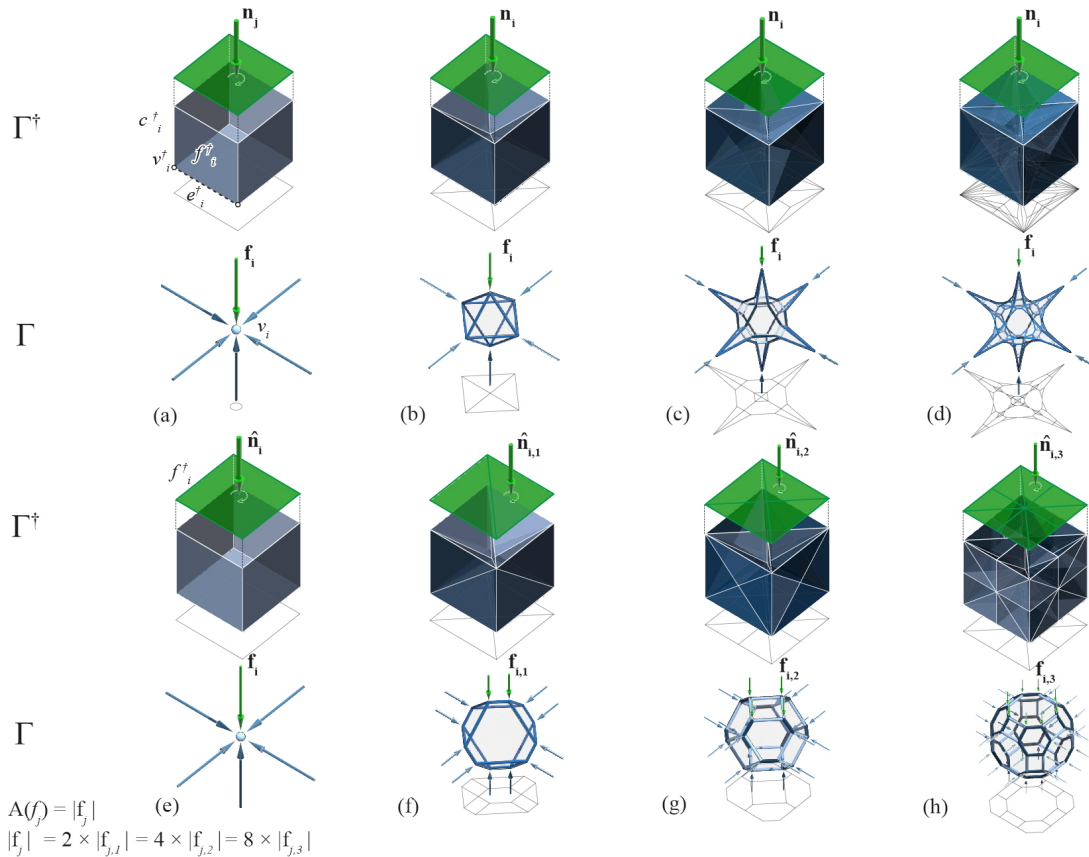
Figure 2: Different types of force diagram's subdivisions in 3DGS result in new form diagrams; (a), (e) a closed cube as a force diagram represents a node in equilibrium; (a-d) internal subdivision of a force diagram without subdividing the global faces; (e-h) subdivision of a force diagram while subdividing the external faces and extruding inside.

and the form finding is achieved by an iterative subdivision of the force diagram across its labyrinths [2]. But this iterative process is computationally very expensive, preventing interactive exploration of various forms for an initial force diagram. The methodology starts with identifying three sets of labyrinth graphs for the initial force diagram and immediately visualizing their form diagrams as smooth and continuous surfaces. Followed by exploring and finalizing the desired form, the force diagram will be subdivided across the desired labyrinth graph to result in a shellular funicular form diagram (Figure 1). The paper concludes by evaluating the mechanical performance of continuous shellular structures in comparison with their discrete counterparts.

Keywords: 3D graphic statics, shellular, structure, form finding, Catmull-Clark algorithm.

1. Introduction
This section is divided to three main parts; first the authors explain the geometry of shell cellular (shellular) structures, then an introduction to the graphic statics as a geometric form finding technique will be given, and finally the shellular structures in the context of graphic statics will be introduced.
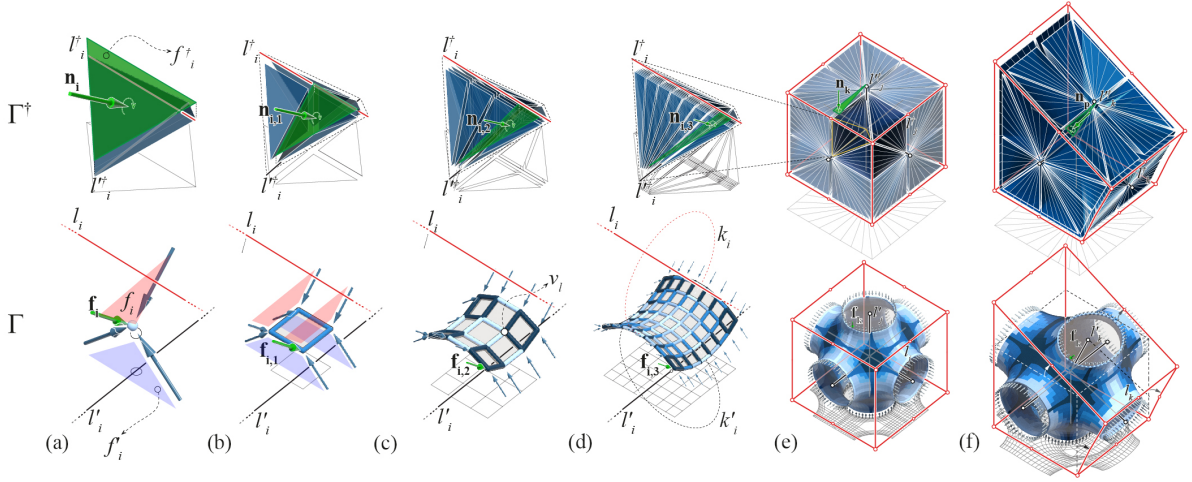
Figure 3: Iterative subdivision of a tetrahedron as a force diagram approximates a discrete surface with anticlastic curvature (a-d) as the form diagram. Using this subdivision between specific labyrinth graphs, one can design a shellular funicular structure (e) and use the labyrinths as control handles to manipulate the structure (f).

1.1. Shellular structures

Shell structures as thin, curved plate structures are shaped to transfer forces via compression, tension and shear stresses that act in the plane of the surface. These structures have a lot of applications in design, construction, and science [3–5]. Shell cellular (shellular) structures as a category of cellular structures are composed of continuous smooth-curved shells. The geometry of these structures includes a surface with the least amount of material filling the space, called minimal surface [6]. The geometry of these surfaces in nature (e.g., soap film) have inspired many architects and engineers to design lightweight structures[7]. In each point of the geometry of minimal surfaces, they have zero mean curvature ($H = k_1 \times k_2$) and negative Gaussian curvature ($G = k_1 \times k_2 < 0$, considering k_1 and k_2 as the principal curvatures of the surface) [8]. Due to the high surface-to-volume ratio and specific morphology, shells with the geometry of these surfaces have shown better mechanical performance, compared to the other cellular structures (e.g., strut-based cellular structures) [2, 9, 10].

1.2. Graphic statics

Utilizing graphic statics, as an intuitive structural design method, one can design a structure using reciprocal diagrams, while controlling the internal flow of force and the external loading scenario [11–15].Three dimensional graphic statics (3DGS) or polyhedral graphic statics (PGS), as an extension of two dimensional graphic statics (2DGS), enables the user to design axially-loaded structures in 3D in which no bending occurs [16–19]. A clear relation between the *form* and *force* diagrams enables the designer to represent the equilibrium of a 3 dimensional node (form diagram) using a closed polyhedron (force diagram) (Figure 2a). Each edge e_i or force f_i in the form diagram is perpendicular to the corresponding face $f_i^\dagger$ in the force diagram. The form diagram represents the geometry of the structure combined with the reaction forces and applied loads, while the force diagram represents the equilibrium of internal and external forces [16]. In this paper, the form diagram is denoted by Γ and the force diagram by $\Gamma^\dagger$. Moreover, the force diagram's topological elements are denoted by † superscript (Figure 2). These diagrams consist of vertices v_i, edges e_i, faces f_i, and cells c_i. Each vertex, edge, face, and cell ($v_i^\dagger, e_i^\dagger, f_i^\dagger, c_i^\dagger$) in

the force diagram corresponds to a cell, face, edge, and vertex (v_i, e_i, f_i, c_i) in the form diagram [16]. In these structures, the magnitude of the force in each strut member (f_i) in the form diagram is proportional to the area of the corresponding face in the force diagram (A_{f_i}). In this technique, by applying different subdivision to a force diagram, one is able to design various cellular strut-based structures in equilibrium (Figure 2a-h). Adding thickness to each edge of the form diagram proportional to the area of its corresponding face results in a strut-based cellular funicular structure (CFS) [20].

1.3. Shellular structures in the context of graphic statics (shellular funicular structures)

Increasing the number of subdivisions in the force diagram results in a form diagram with smaller edges and distributed forces in the members (Figure 2a-d and e-f). This process can finally result in the edges with near zero-length, approximating a surface as a form diagram. Specific subdivision techniques in PGS can approximate surfaces with anticlastic or synclastic curvatures as form diagrams [2]. Figure 3a displays a tetrahedron as a force diagram corresponding to a node in equilibrium with two forces upward and two downward as a form diagram (a node with an anticlastic curvature). This tetrahedron is generated by connecting the end points of the two skew lines $l_i^\dagger$ and $l_i'^\dagger$. Dividing these lines into equal segments and establishing a tetrahedron between each two skew segments from each line, subdivides the force diagram into multiple tetrahedrons, resulting in a discrete anticlastic surface as a form diagram (Figure 3a-d) [2, 21]. This type of subdivision is called the *anticlastic subdivision*. These lines ($l_i^\dagger$ and $l_i'^\dagger$) play the role of subdivision axis in the force diagram and the curvature axis in the form diagram (Figure 3d). These lines are parts of two connectivity graphs, named *labyrinths*, connecting two segregated regions, divided by the anticlastic surface in between [22]. Using the *anticlastic subdivision* technique, one can design an anticlastic polyhedral surface, named a Shellular Funicular Structure (SFS) [1]. The labyrinths as the subdivision axes in the form and the control handles in the force, facilitate the design process and manipulation of the SFSs form-finding technique [21].

1.4. Problem statement and objectives

Although one is able to design various shellular funicular structures by designing different set of labyrinths, the anticlastic subdivision in this process is computationally expensive, preventing interactive exploration of various forms for an initial force diagram. In this article, a new method will be introduced to design various forms from an initial force diagram and to approximate their geometry using a smoothing algorithm. The methodology starts with identifying three sets of labyrinth graphs for the initial force diagram and immediately visualizing their form diagrams as smooth and continuous surfaces. Followed by exploring and finalizing the desired form, the force diagram will be subdivided across the desired labyrinth graph to result in a shellular funicular form diagram (Figure 1). The paper concludes by evaluating the mechanical performance of continuous shellular structures in comparison with their discrete counterparts.

2. Methodology

This section is divided to three main parts; first a technique will be introduced to translate a cellular funicular structure to its shellular counterpart, then a novel method will be introduced by which the user can design three different labyrinth graphs for an initial tetrahedralized force diagram, and finally a method for visualizing a two-manifold form diagram using the Catmull-Clark algorithm will be explained.
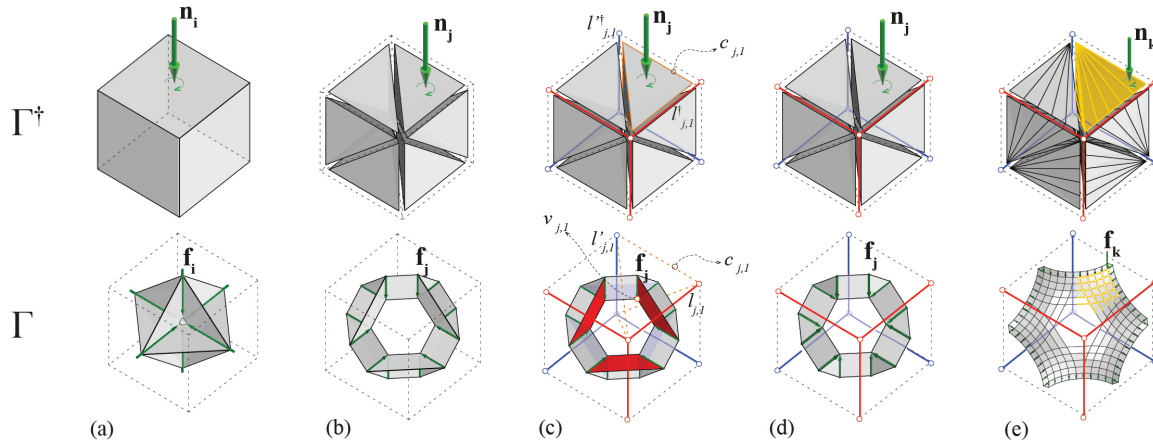
Figure 4: The process of translating a cellular funicular to a shellular funicular structure in PGS; a. initial force and form diagrams, b. tetrahedralizing the force diagram, c. finding the labyrinth graphs, d. removing the faces corresponding to the labyrinths in the form diagram, and e. applying an anticlastic subdivision to the labyrinth graphs.

2.1. Translating a cellular funicular structure (CFS) to a shellular funicular structure(SFS)

Translating the geometry of a cellular funicular structure to a shellular funicular structure in the context of graphic statics requires subdividing the force diagram such that each vertex v_i connected to a group of edges e_i and faces f_i converts to a discrete anticlastic patch with smaller edges, approximating a discrete anticlastic surface.

In the SFS design process, there are three main principles that are needed to be considered;

1. each pair of labyrinths in the form diagram should form a tetrahedron in between, corresponding to an anticlastic node in the form diagram,

2. the force diagram includes two sets of labyrinths and each tetrahedron in the force diagram should only include one labyrinth edge from each set which is in a skew position to the other,

3. each labyrinth's edge in the force diagram can be connected to the labyrinth edges from the same set, assuring that the resulting surface (form diagram) will divide the space into two subspaces.

The process of translating a CFS to a SFS starts with initial funicular diagrams (form and force diagrams) that are designed with the Polyframe software or the 3DGS's WebTool (Figure 4a) [23, 24]. According to the first principle that is mentioned above, each force diagram should only include tetrahedrons, resulting in 4-valency vertices or vertices that are connected to 4 edges in the form diagram which represent an anticlastic curvature (Figure 4b). After subdividing the force diagram to a group of tetrahedrons (*tetrahedralization*), two skew edges from each tetrahedron are selected as the labyrinths' edges (Figure 4c). This step will be processed according to the SFSs' main principles, assuring that each tetrahedron only includes two labyrinths' edges and each labyrinth's edge is only connected to the labyrinth's edges from the same set [25]. It is important to notice that one may result in three different labyrinths' graphs
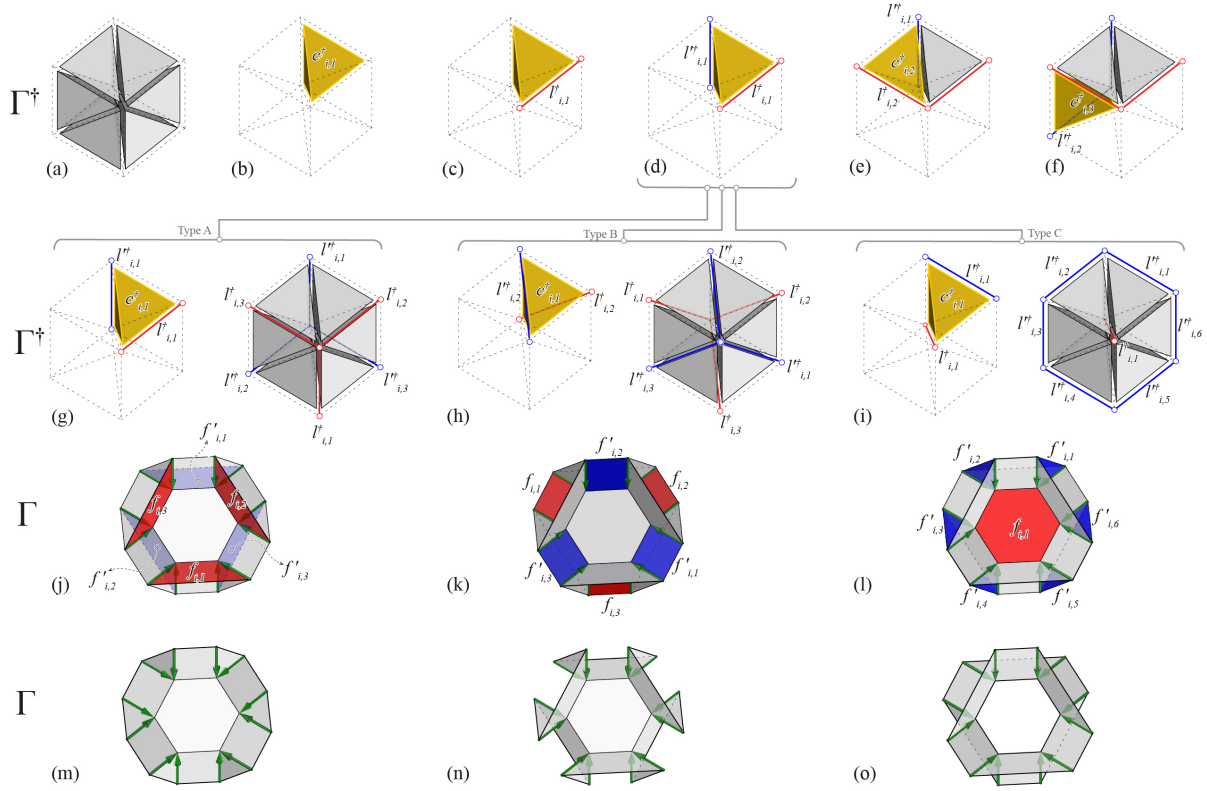
Figure 5: The process of finding a labyrinths' graph in a tetrahedralized force diagram (a-f) and 3 different types of graphs resulting from this algorithm (g, h, i) along with the corresponding form diagrams (j, k, l) and removing the faces corresponding to the labyrinths' graphs.

in this step which gives the user the opportunity to choose between them. This step has been explained in detail in section 2.2. Each of the labyrinths' graphs in the force diagram correspond to a group of faces in the form diagram. Removing these faces from the form diagram results in a two-manifold form diagram in which each edge is only connected to two faces (Figure 4d). Although the resulted form diagram is a two-manifold geometry, it still needs to be subdivided to a certain degree in order to result in a smooth shellular funicular form diagram. This step can be done in two ways, either the user can subdivide the force diagram using an *anticlastic subdivision* that is explained in section 1.3 or can use a smoothing algorithm which has been explained in section 2.3 (Figure 4e).

2.2. Finding three different labyrinth graphs for an initial tetrahedralized force diagram

After tetrahedralizing the force diagram, two sets of labyrinth graphs are needed to be selected each edge of which are in a skew position to the other one. Figure 5 displays the process of finding labyrinth graphs in a tetrahedralized force diagram. The process starts with a cube as a global force diagram that is tetrahedralized to six tetrahedrons (Figure 5a). Starting from a random cell $c^\dagger_{i,1}$, two labyrinth edges $l^\dagger_{i,1}$ and $l'^\dagger_{i,1}$ which are in a skew position together are selected (Figure 5b-d). Next, one of the neighbor cells will be selected which shares the labyrinth edge $l'^\dagger_{i,1}$ with $c^\dagger_{i,1}$. Then, the second skew edge to $l'^\dagger_{i,1}$ ($l^\dagger_{i,2}$) will be selected (Figure 5e). This process will be continued until all the cells are passed (Figure 5f,g). Figure 5g displays the labyrinth graphs that are selected for the initial force diagram. But we
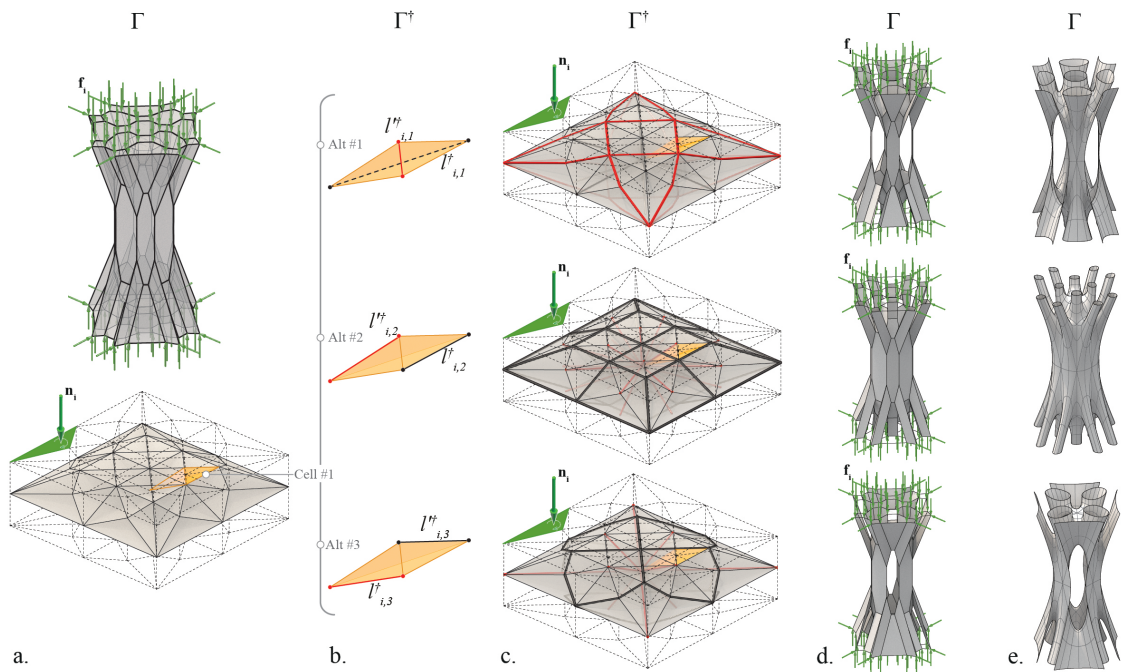
Figure 6: The process of designing the geometry of shellular funicular structures for a boundary condition comparable to a column (a-d) and approximating it using the Catmull-Clark algorithm (e).
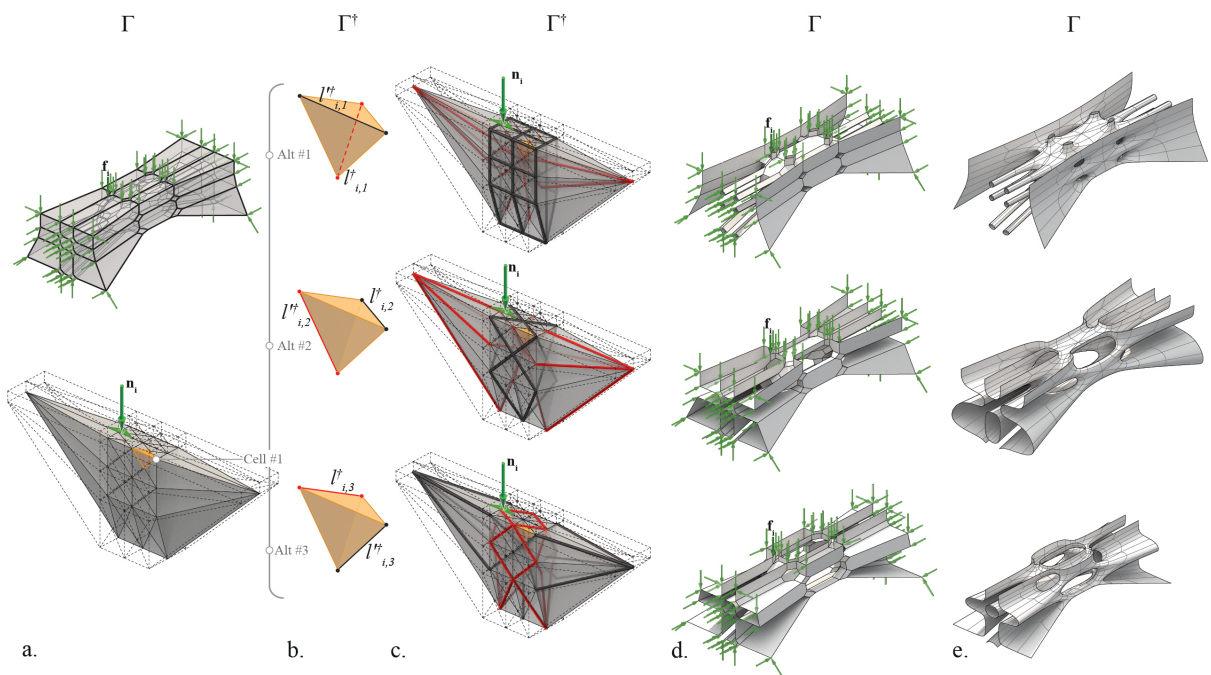

Figure 7: The process of designing the geometry of shellular funicular structures for a boundary condition comparable to a bridge (a-d) and approximating it using the Catmull-Clark algorithm (e).

observe that selecting different pair of labyrinth in the first step would result in new set of labyrinths. In fact, selecting $l'^{\dagger}_{i,2}$ and $l^{\dagger}_{i,2}$ or $l'^{\dagger}_{i,3}$ and $l^{\dagger}_{i,3}$ as the labyrinth edges of the cell $c^{\dagger}_{i,1}$ would result in new labyrinth graphs which finally generates new form diagrams. Since each tetrahedron has six edges or three skew pairs, we result in three different labyrinth edges for each tetrahedralized force diagram. It is important to notice that in some situations, due to a specific edge-cell connectivity (when each edge in a tetrahedralize force diagram is connected to the odd number of cells) the process that is explained above only results in one solution [25]. After finding the labyrinth graphs, one needs to remove the faces in the form diagram corresponding to the labyrinth graph's edges. In fact each edge in the force diagram corresponds to a face in the form diagram. By removing the faces $f_{i,1}$, $f_{i,2}$, $f_{i,3}$, $f'_{i,1}$, $f'_{i,2}$ and $f'_{i,3}$ in the form diagram corresponding to the edges $l^{\dagger}_{i,1}$, $l^{\dagger}_{i,2}$, $l^{\dagger}_{i,3}$, $l'^{\dagger}_{i,1}$, $l'^{\dagger}_{i,2}$ and $l'^{\dagger}_{i,3}$ respectively in the force diagram, the first two-manifold form diagram will be generated (Figure 5g, j, m). Similarly, eliminating faces correspond to the labyrinth edges in Figure 5k and l also result in new two manifold form diagrams (Figure 5n and o).

Similar to the process that is explained above, for each tetrahedralized force diagram, if there is no singularity in the system (i.e., all the edges in the force diagram are connected to an even number of cells) [25], one can find three different labyrinth graphs corresponding to three different shellular form diagrams.

Figures 6 and 7 display processes of finding labyrinth graphs for two tetrahedralized force diagrams that are designed for different loading scenarios. Figure 6a, displays force and form diagrams of a cellular system that is constrained from the top and the bottom, similar to the loading condition of a column. After selecting a random cell from the force diagram, there are three different labyrinth sets for the cell each of which comprising two edges in a skew position to each other (Figure 6b). Next, all the neighbor cells will be parsed and three different labyrinth graphs will be determined (Figure 6c). Each of these sets in the force diagram corresponds to a group of faces in the form diagram. Followed by removing the corresponding faces in the force diagram, one results in a two-manifold form diagram (Figure 6d). Similarly, Figure 7a-d illustrates the process of finding the labyrinth graphs for a new tetrahedralized force diagram that is designed for a new boundary condition. This structure is constrained on two sides and the top, comparable to the loading condition of a bridge.

Although applying an *anticlastic subdivision* to each pair of labyrinth edges in the force diagram results in a smoother version of the form diagram (section 1.3), this process is computationally expensive and time consuming. Therefore, there is a need for a faster smoothing algorithm to visualize the smooth versions of the form diagrams so the user can select the desired form diagram and subdivide it (Figures 6e and 7e). Section 2.3 illustrates the mentioned smoothing algorithm in details.

2.3. Visualizing or subdividing a two-manifold form diagram to a smooth SFS

After resulting in a two-manifold form diagram, one needs to apply an anticlastic subdivision to the force diagram to generate a semi-smooth shellular funicular form diagram. This process increases the number of topological elements of the form and the force diagrams and is computationally expensive. Therefore, it makes it challenging for the user to explore different alternatives. Furthermore, to develop an interactive procedure for this technique, we need to generate the form quickly. Hence, we require an smoothing algorithm which is fast and effective. Smoothing is the process of dividing the polygons of a 3-dimensional mesh into smaller polygons by relocating the mesh vertices to new locations such that

elements incident at that vertex have improved quality. This procedure repositions the vertices based on adjacent vertices and is done iteratively for each vertex until the desired mesh quality is reached or it
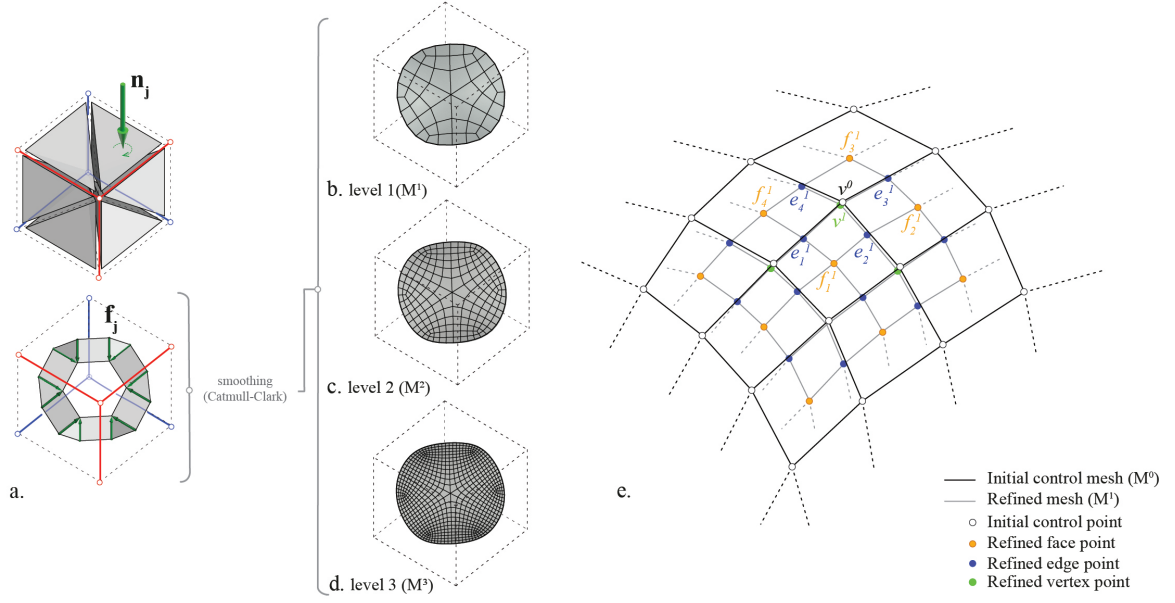
Figure 8: The process of smoothing a discrete anticlastic patch that is designed in the context of graphic statics (a) and applying three levels of smoothing to it using the Catmull-Clark algorithm (b-d), along with the Catmull-Clark subdivision process for a rectangular control-point mesh (e).

cannot be improved further [26]. The Catmull-Clark algorithm is a technique to create curved surfaces using subdivision surface modeling [27]. The algorithm starts with an arbitrary mesh called the *control mesh* (M^0). In the SFS's method, the two-manifold form diagram resulted from the tetrahedralized force diagram with its labyrinths plays the role of the control mesh (Figure 8a). In the first iteration, each face of this mesh is subdivided to a collection of quadrilateral subfaces, resulting in the mesh M^1(Figure 8b). In this process, a face with n edges is split into n quadrilaterals. Repeating the application of the same subdivision procedure results in the next meshes (e.g., $M^2, M^3, ...$) which are the smoother versions of the initial control mesh (Figure 8). In this procedure, each vertex of the mesh M^{i+1} is associated with either a vertex, edge or a face of M^i, called vertex point(v), edge point (e) and face point (f) respectively. Each face point f_j^{i+1} is the centroids of the vertices of the face. An edge point e_j^{i+1} is computed as;

$$e_j^{i+1} = \frac{v^i + e_j^i + f_{j-1}^{i+1} + f_j^{i+1}}{4}.$$

(1)

In Figure 8e, the subscripts are taken modulo the valence of the vertex v_0 (as the number of edges incident to the vertex). Moreover, a vertex point v_i is computed as;

$$v^{i+1} = \frac{n-2}{n}v^i + \frac{1}{n^2}\sum_j e_j^i + \frac{1}{n^2}\sum_j f_j^{i+1} [28].$$

(2)

With this technique, the user is able to smooth a two-manifold geometry without applying an *anticlastic*
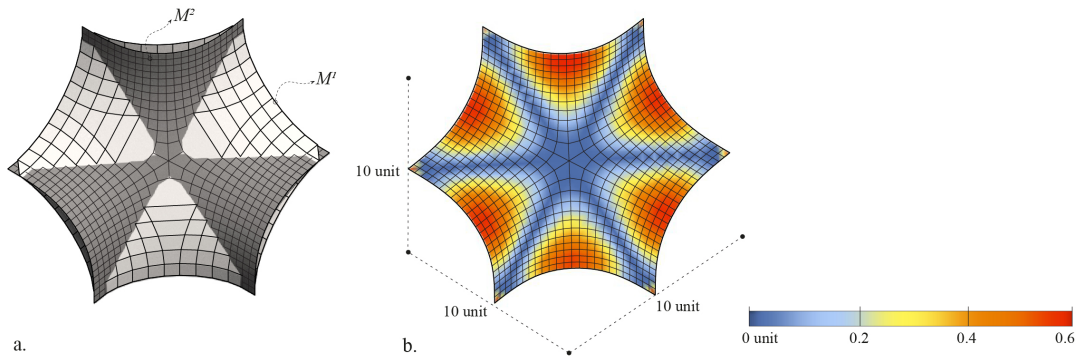
9

Figure 9: Comparing the geometry of two meshes that are subdivided in the context of graphic statics (M^1) and using the Catmull-Clark subdivision (M^2) by superimposing their geometry (a) and evaluating the distance between two meshes and mapping the distance field on the mesh that is designed using the Catmull-Clark algorithm (b).

subdivision to the force diagram. But the question here is whether this geometry is comparable to the geometry of a shellular funicular structure that is generated via an *anticlastic subdivision* in PGS. Figure 9a displays a superimposition of the mesh M^1 as the form diagram in PGS after applying three degree of anticlastic subdivision to it, and mesh M^2 as the continuous approximation of a two manifold form diagram after applying the Catmull-Clark subdivision. Comparing the geometry of these meshes, we observe that their curvature do not match perfectly (Figure 9b). Therefore, the structural capacity of the specimen that is approximated with the Catmull-Clark algorithm might not be comparable to the one that is generated in PGS.

3. Comparing the mechanical performance shellular funicular structures generated in PGS and their continuous approximation

In this section, a numerical structural analysis is performed to study the mechanical behavior of three shellular funicular structures shown in Figure 10a-c. The first specimen is named *subd1-not-smooth* which is the same two-manifold form diagram before smoothing that is generated in Figure 6d, bottom (Figure 10a). The second specimen is named *subd1-smooth* which is the smooth version of the previous specimen via Catmull-Clark algorithm (Figure 10b). The third specimen is named *subd5-smooth* which is the smooth version of the first specimen via the *anticlastic subdivision*. In fact this specimen is subdivided to the fifth level in the polyhedral graphic statics' context (PGS), meaning that each tetrahedron in the force diagram of the first specimen is subdivided to 25 tetrahedrons corresponding to 25 valency four vertices connect to each other in the form diagram. These specimens are made out of structural steel and they have identical volume density. A tetrahedral mesh consist of around half a million elements are generated for all specimens with similar boundary condition, loading speed and type of elements. After the finite elements analysis, we observe that the smooth specimens have better structural performance since they distribute the stress evenly in the structure compared to the specimen without smoothing. Comparing the structural performance of the smooth specimens, the *subd5-smooth* specimen has better structural performance and can distribute the stress in the structure more consistent compared to the *subd1-smooth* since we have already assured that in this specimen, the thrust lines are located inside the thickness of the material. But in the second specimen, some part of the thrust lines before applying the Catmull-Clark subdivision is outside of the thickness of the material. Therefore, in order to assure that the smoothing process is structurally dependable, one needs to first smooth the form diagram in the
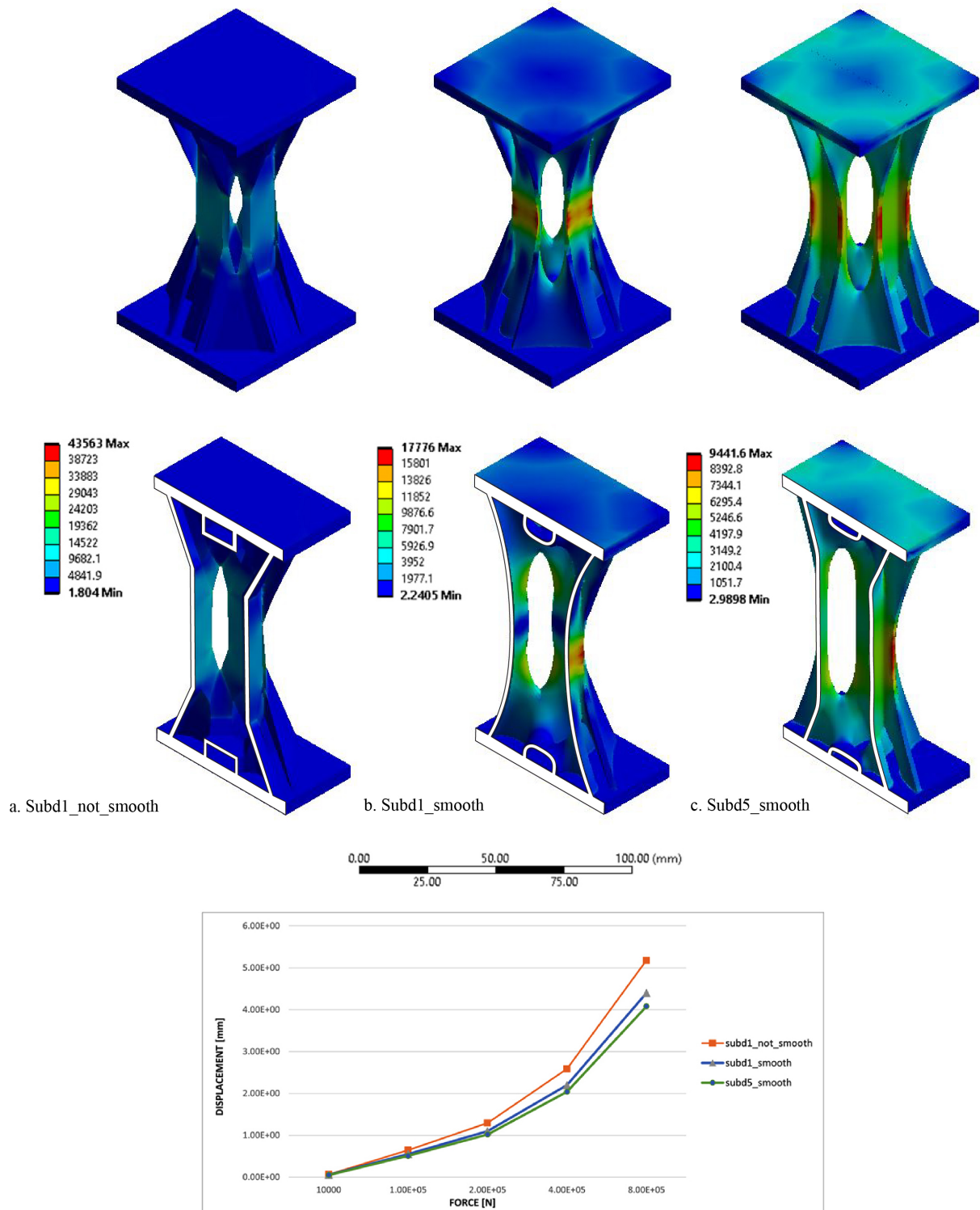
Figure 10: Mises stress contour of the subdivision 1 before smoothing (a), the subdivision 1 after smoothing (b), and the subdivision 5 after smoothing (c), with the same volume density along with comparing the load-displacement curves of the specimens.

context of graphic statics using the *anticlastic subdivision* to a certain degree and then apply the Catmull-Clark subdivision. By this, one can make sure that the thrust lines of the structure are located inside the thickness of the material. Although it is worth to mention that this operation depend on the thickness of the material. Therefore, determining the minimum thickness for a specimen depends on its thrust lines, whether they are located in the thickness of the material or not. But the Catmull-Clark subdivision is a fast and effective algorithm which can help the user to visualize the smooth version of the form quickly.

4. Conclusion and future directions

This paper discussed a novel technique for exploring different design alternatives for shellular funicular form diagrams. The authors showed that it is possible to identify three sets of labyrinth graphs for the initial force diagram, resulting in three different two-manifold form diagrams. Furthermore, a smoothing algorithm is explored for visualizing the smooth version of the form diagrams quickly, enabling the user to do interactive explorations with the structure. Finally, the paper concluded by evaluating the mechanical performance of continuous shellular structures (that are subdivided via Catmull-Clark subdivision) in comparison with their discrete counterparts that are subdivided with the *anticlastic subdivision* in the context of graphic statics. In future, the authors intend to use this technique to develop an interactive application for generating shellular funicular structures in the context of graphic statics.

References

[1] M. Akbari, A. Mirabolghasemi, M. Bolhassani, A. Akbarzadeh, and M. Akbarzadeh, "Strut-based cellular to shellular funicular materials," *Advanced Functional Materials*, p. 2109725, 2022.

[2] M. AKBARI, M. AKBARZADEH, and M. BOLHASSANI, "From polyhedral to anticlastic funicular spatial structures," in *Proceedings of IASS Symposium*, 2019.

[3] T. Teng, M. Jia, and J. E. Sabin, "The designing of epithelial cell inspired-brick inmasonry shell system," 2020.

[4] T. Teng and J. Sabin, "The design and 4d printing of epithelial cell-inspired programmable surface geometry," 2021.

[5] S. Adriaenssens, P. Block, D. Veenendaal, and C. Williams, *Shell structures for architecture: form finding and optimization*. Routledge, 2014.

[6] W. Meeks III and J. Pérez, "The classical theory of minimal surfaces," *Bulletin of the American Mathematical Society*, vol. 48, no. 3, pp. 325–407, 2011.

[7] B. Burkhardt, "Natural structures-the research of frei otto in natural sciences," *International journal of space structures*, vol. 31, no. 1, pp. 9–15, 2016.

[8] D. Hilbert and S. Cohn-Vossen, *Geometry and the Imagination*, vol. 87. American Mathematical Soc., 2021.

[9] S. C. Han, J. W. Lee, and K. Kang, "A new type of low density material: Shellular," *Advanced Materials*, vol. 27, no. 37, pp. 5506–5511, 2015.

[10] S. C. Han, J. M. Choi, G. Liu, and K. Kang, "A microscopic shell structure with schwarz's d-surface," *Scientific reports*, vol. 7, no. 1, pp. 1–8, 2017.

[11] J. C. Maxwell, "On Reciprocal Figures and Diagrams of Forces," *Philosophical Magazine Series 4*, vol. 27, no. 182, pp. 250–261, 1864.

[12] W. J. M. Rankine, "Principle of the Equilibrium of Polyhedral Frames," *Philosophical Magazine Series 4*, vol. 27, no. 180, p. 92, 1864.

[13] L. L. Beghini, J. Carrion, A. Beghini, A. Mazurek, and W. F. Baker, "Structural Optimization Using Graphic Statics," *Structural and Multidisciplinary Optimization*, vol. 49, no. 3, pp. 351–366, 2013.

[14] L. Cremona, *Graphical Statics: Two Treatises on the Graphical Calculus and Reciprocal Figures in Graphical Statics. Translated by Thomas Hudson Beare*. Oxford: Clarendon Press, 1890.

[15] K. Culmann, *Die Graphische Statik*. Zürich: Verlag Meyer und Zeller, 1864.

[16] M. Akbarzadeh, *3D Graphic Statics Using Reciprocal Polyhedral Diagrams*. PhD thesis, ETH Zurich, Zurich, Switzerland, 2016.

[17] Y. Lu, M. Cregan, P. Chhadeh, A. Seyedahmadian, M. Bolhassani, J. Schneider, J. Yost, and M. Akbarzadeh, "All glass, compression-dominant polyhedral bridge prototype: form-finding and fabrication," in *Proceedings of IASS Symposium and Spatial Structures Conference 2020/21, Inspiring the next generation*, (Guildford, UK), August 23-27 2021.

[18] H. Zheng, M. Hablicsek, and M. Akbarzadeh, "Lightweight structures and the geometric equilibrium in dragonfly wings," *International Association of Shell and Spatial Structures*, 2021.

[19] H. Zheng, X. Wang, Z. Qi, S. Sun, and M. Akbarzadeh, "Generating and optimizing a funicular arch floor structure," *Association of Computer-Aided Architectural Design*, 2021.

[20] M. Akbarzadeh, A. Tabatabaie Ghomi, M. Bolhassani, M. Akbari, A. Seyedahmadian, J. Sun, H. Yao, , J. Miziumski, and K. Papalexiou, "Saltatur: Node-based assembly of funicular spatial concrete," in *Proceedings of the 40th Annual Conference of the Association for Computer-Aided Design in Architecture (ACADIA)*, 2021.

[21] M. Akbari, A. Mirabolghasemi, H. Akbarzadeh, and M. Akbarzadeh, "Geometry-based structural form-finding to design architected cellular solids," in *Symposium on Computational Fabrication*, pp. 1–11, 2020.

[22] W. Fischer and E. Koch, "Genera of minimal balance surfaces," *Acta Crystallographica Section A: Foundations of Crystallography*, vol. 45, no. 10, pp. 726–732, 1989.

[23] A. Nejur and M. Akbarzadeh, "Polyframe, efficient computation for 3d graphic statics," *Computer-Aided Design*, vol. 134, p. 103003, 2021.

[24] H. Chai and M. Akbarzadeh, "Web-based Interactive Polyhedral Graphics Statics Platform," in *Proceedings of the IASS Annual Symposium 2020/21*, (Surrey,UK), 2021.

[25] M. Akbari, Y. Lu, and M. Akbarzadeh, "From design to the fabrication of shellular funicular structures," in *Proceedings of the Association for Computer-Aided Design in Architecture (ACADIA)*, 2021.

[26] T. Prasad, *A comparative study of mesh smoothing methods with flipping in 2D and 3D*. PhD thesis, Rutgers University-Camden Graduate School, 2018.

[27] E. Catmull and J. Clark, "Recursively generated b-spline surfaces on arbitrary topological meshes," *Computer-aided design*, vol. 10, no. 6, pp. 350–355, 1978.

[28] T. DeRose, M. Kass, and T. Truong, "Subdivision surfaces in character animation," in *Proceedings of the 25th annual conference on Computer graphics and interactive techniques*, pp. 85–94, 1998.